The Astrophysical Journal, 781:118 (5pp), 2014 February 1 doi:10.1088/0004-637X/781/2/118

INTERMITTENT DUST MASS LOSS FROM ACTIVATED ASTEROID P/2013 P5 (PANSTARRS)

F. Moreno[1], J. Licandro[2,3], C. Álvarez-Iglesias[2,3,4], A. Cabrera-Lavers[2,3,4], and F. Pozuelos[1]
[1] Instituto de Astrofísica de Andalucía, CSIC, Glorieta de la Astronomía s/n, E-18008 Granada, Spain; fernando@iaa.es
[2] Instituto de Astrofísica de Canarias, c/Vía Láctea s/n, E-38200 La Laguna, Tenerife, Spain
[3] Departamento de Astrofísica, Universidad de La Laguna (ULL), E-38205 La Laguna, Tenerife, Spain
[4] GTC Project, E-38205 La Laguna, Tenerife, Spain
Received 2013 November 29; accepted 2013 December 16; published 2014 January 16

ABSTRACT

We present observations and models of the dust environment of activated asteroid P/2013 P5 (PANSTARRS). The object displayed a complex morphology during the observations, with the presence of multiple tails. We combined our own observations, all made with instrumentation attached to the 10.4 m Gran Telescopio Canarias on La Palma, with previously published *Hubble Space Telescope* images to build a model aimed at fitting all the observations. Altogether, the data cover a full three month period of observations which can be explained by intermittent dust loss. The most plausible scenario is that of an asteroid rotating with the spinning axis oriented perpendicular to the orbit plane and losing mass from the equatorial region, consistent with rotational break-up. Assuming that the ejection velocity of the particles ($v \sim 0.02$–0.05 m s^{-1}) corresponds to the escape velocity, the object diameter is constrained to ∼30–130 m for bulk densities 3000–1000 kg m^{-3}.

Key words: methods: numerical – minor planets, asteroids: individual (P/2013 P5 (PANSTARRS))

Online-only material: color figures

1. INTRODUCTION

Activated asteroid P/2013 P5 (PANSTARRS) was discovered by Pan-STARRS survey as a 21st magnitude comet on 2013 August 15.50 (Micheli et al. 2013). This object has a typical inner-belt asteroid orbit but displays a cometary-like tail, so it can be classified as a main-belt comet (MBC). The object shares similar orbital elements with previously discovered disrupted asteroid P/2010 A2 (LINEAR; Jewitt et al. 2010; Snodgrass et al. 2010; Moreno et al. 2013), both belonging to the Flora collisional family. The origin of the activity taking place in the MBCs is unknown for most of the those objects. While some have been associated with impulsive events, such as collisions with another body or rotational break-up, others are most likely linked to water–ice sublimation. For reviews on those objects and the likely mechanisms involved in their activity, see, e.g., Hsieh & Jewitt (2006), Bertini (2011), and Jewitt (2012).

A series of stunning images from the *Hubble Space Telescope* (*HST*; Jewitt et al. 2013) at two epochs reveal the asteroid as a multiple-tailed object. Using the Finson–Probstein formalism, these tails have been associated with a series of ejection events at different dates, and the likely cause of the activity has been linked to a rotational disruption. In this paper, we present our own data, which were acquired two months after the *HST* observations, and combine them with the *HST* data. Our aim is then to monitor the activity scenario during a longer time frame and, mostly, to characterize the dust activity in terms of the time variation of the mass loss, particle size distribution, and ejection velocities. Models mimicking an equatorial mass loss from the object have been incorporated in an attempt to investigate if a rotational disruption could be compatible with the ejection scenario.

2. OBSERVATIONS AND DATA REDUCTION

Images of P/2103 P5 through the Sloan r' and g' filters were recorded under photometric and excellent seeing conditions (0.″8–0.″9) on the nights of 2013 October 7 and 2013 November 8 (only r' images). We used the Optical System for Image and Low Resolution Integrated Spectroscopy (OSIRIS) camera-spectrograph (Cepa et al. 2000; Cepa 2010) at the Gran Telescopio Canarias (GTC). The OSIRIS instrument consists of two Marconi CCD detectors, each with 2048 × 4096 pixels and a total unvignetted field of view of 7.′8 × 7.′8. The plate scale was 0.″127 pixel^{-1}, but we used a 2 × 2 pixel binning in order to improve the signal-to-noise ratio, so that the spatial resolution of the images becomes 222 km pixel^{-1} and 270 km pixel^{-1} at the observation dates. The images were bias and flat-field corrected using standard techniques, and calibrated in flux using standard stars. A sequence of five images per filter were obtained. An average image was then obtained from the available images by shifting and stacking the frames with respect to a reference frame by taking into account the object's sky motion. We estimate that as a result of both the flux calibration and the stacking procedure, the total flux uncertainty in the combined images is ∼0.1 mag. The final combined images are shown in Figure 1. The log of the observations is shown in Table 1. In that table, the apparent (m) and absolute (H) magnitudes of a region of 10 pixel aperture radius (2.″5 diameter) centered on the asteroid optocenter of each image is given. The absolute magnitude is given as $H = m - 2.5\log(\Delta r_h) - \Phi(\alpha)$, where Δ and r_h are the geocentric and heliocentric distances of the asteroid, and $\Phi(\alpha)$ is the phase function, which is assumed to be that of an S-type asteroid, as most objects in the inner asteroid belt. The quantity $\Phi(\alpha)$ is computed using the Bowell et al. (1989) formalism, using a phase function parameter $g = 0.25$, which is typical of S-type asteroids, the most common objects in the inner belt. The phase terms become $\Phi(17.^\circ7) = -0.81$ on October 7, and $\Phi(27.^\circ0) = -1.07$ on November 8, and the absolute magnitude $H_{r'}$ converges to the value $H_{r'} = 18.0 \pm 0.1$ in both dates. To compare this value to the reported H_V by Jewitt et al. (2013; $H_V = 18.69$ on September 10 and $H_V = 18.54$ on September 23), we need a transformation from r' to V magnitudes. Using the transformation equations of Fukugita et al. (1996) and the magnitude of the Sun in the standard Johnson–Cousins filter ($V_\odot = -26.75$; Cox 2000), we derive $r'_\odot = -26.96$. If the object follows a spectral dependence on wavelength similar to that of the Sun within the

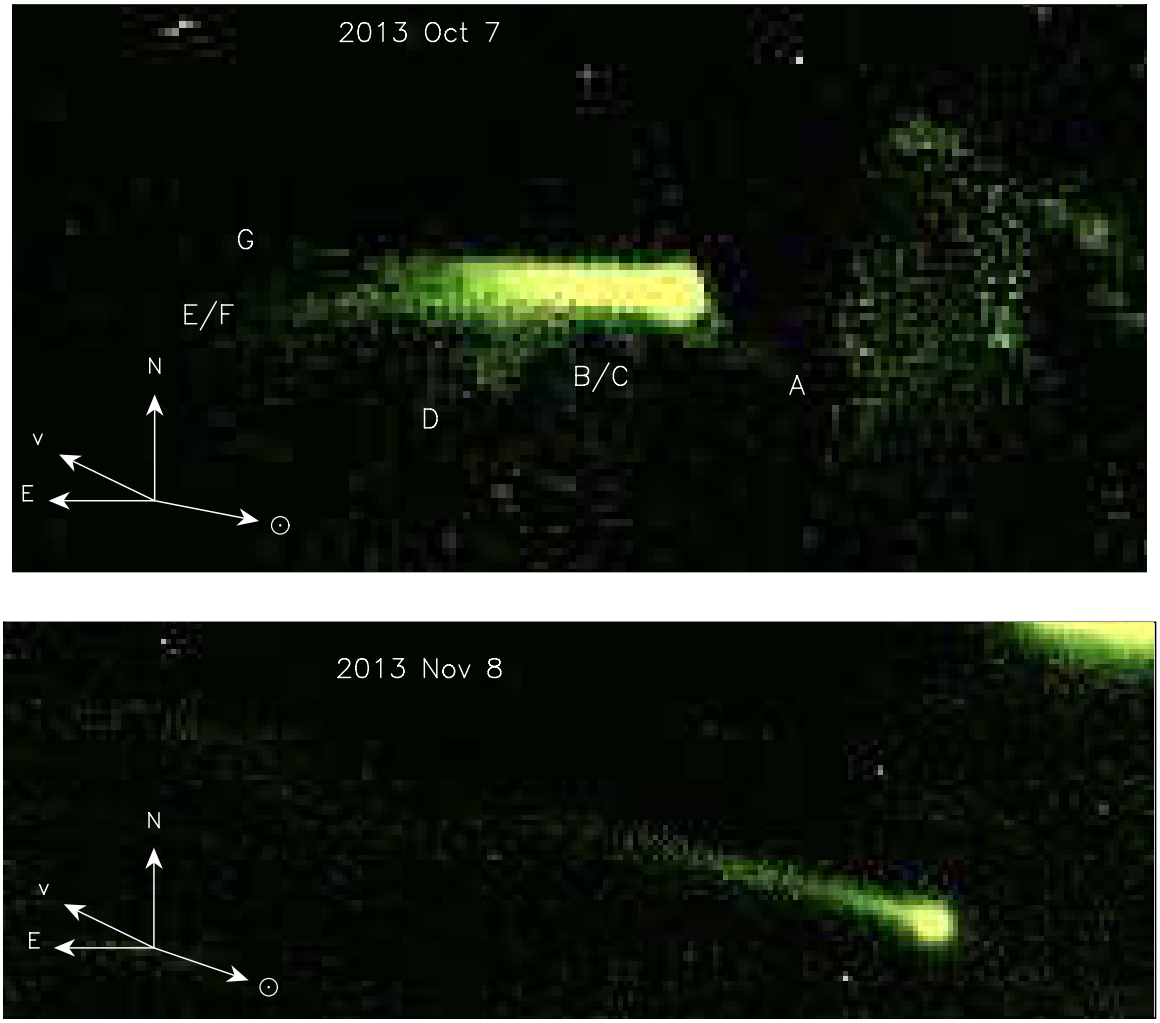

Figure 1. Stacked r' Sloan OSIRIS@GTC images of P/2013 P5 on the nights of UT 2013 October 7 (upper panel) and 2013 November 8 (lower panel). The dimensions of the upper and lower images are 35,488 × 17,744 km and 61,939 × 21,275 km, respectively. In the upper panel the different tails are marked. The nomenclature follows that of Jewitt et al. (2013). Tails marked as B/C and E/F are actually a blend of tails B and C, and E and F, respectively, as displayed in Figure 1 of Jewitt et al. (2013); see also Figure 2 in this paper. Note that tail G is the youngest tail and does not appear in the *HST* observations. The directions of celestial north and east are indicated, as well as the direction to the Sun and the asteroid velocity vector.

(A color version of this figure is available in the online journal.)

Table 1
Log of the Observations

Date (UT)	r_h (AU)	Δ (AU)	α (°)	δ (°)	m	H
2013 Oct 7 22:18	2.077	1.204	17.7	−4.10	$g' = 21.3 \pm 0.1$	18.5 ± 0.1
2013 Oct 7 22:26	2.077	1.204	17.7	−4.10	$r' = 20.8 \pm 0.1$	18.0 ± 0.1
2013 Nov 8 21:04	2.038	1.462	27.0	−2.68	$r' = 21.5 \pm 0.1$	18.0 ± 0.1

V and r' bandpasses (neutral color), the V magnitudes can be obtained from the r' magnitudes by adding 0.21 mag. Then, we would get $H_V = 18.2$. This would indicate a brightness increase since September 10 of ∼0.5 mag. This result immediately excludes a single event mechanism of dust ejection from the asteroid, as such event would have resulted in a brightness decrease as a function of time. Assuming that the brightness is entirely due to the asteroid and not to the surrounding dust, this would lead to an asteroid diameter of ∼590 m for a geometric albedo of $p_v = 0.29$, typical of Flora family asteroids (Masiero et al. 2013). We will, however, assume that such brightness is entirely associated with the presence of dust surrounding the asteroid, and not to the presence of a nucleus, its contribution to the brightness being negligible. A justification of this hypothesis is given in the Results section on the basis of the low ejection velocities of the dust particles that we found in the modeling procedure.

3. THE MODEL

To perform the analysis of the images, we used our direct Monte Carlo dust tail model, as described in previous works (e.g., Moreno et al. 2012b; Fulle et al. 2010). In that model, we compute the trajectory of a large number of particles after being ejected from an asteroidal or cometary surface. Those particles

move under the sole influence of solar gravity and radiation pressure forces, describing a Keplerian orbit around the Sun. The orbital elements of each ejected particle are functions of the ejection velocity and the β parameter (e.g., Fulle 1989). This parameter can be written as $\beta = C_{\rm pr} Q_{\rm pr}/(2\rho r)$, where $C_{\rm pr} = 1.19 \times 10^{-3}$ kg m^{-2}, $Q_{\rm pr}$ is the radiation pressure coefficient, and ρ is the particle density. The position of each particle in the plane of sky is then computed according to its orbital elements, and its contribution to the tail or coma brightness is evaluated, as a function of its size and geometric albedo. Owing to the many input models, we are forced to set some of them to a specific value. Then, the particles are considered spherical, their density is assumed at $\rho_p = 1000$ kg m^{-3}, and their refractive index is set at $1.88 + 0.71i$, which is typical of carbonaceous composition (Edoh 1983). Using Mie theory, we find that the geometric albedo is $p_v \sim 0.04$, and that the radiation pressure coefficient is $Q_{\rm pr} \sim 1$ for particles of radius $r \gtrsim 1\,\mu$m (Moreno et al. 2012b, their Figure 5). These choices of density and geometric albedo are highly arbitrary, since we do not know their real values, and were made actually to facilitate comparison with other MBCs analyzed, for which we assumed such values (e.g., Moreno et al. 2010, 2013).

We start by assuming an asteroid nucleus which is losing mass from its equator, where centrifugal acceleration is maximum, uniformly in longitude. This would correspond to a mass loss scenario driven by a rotational disruption, as suggested by Jewitt et al. (2013). This introduces three more model parameters to characterize the rotation properties: the orientation of the spinning axis with respect to the orbit plane, which is given by the obliquity, I, and the argument of the subsolar meridian at perihelion, Φ, and the rotational period, P (simple rotation is assumed). The nucleus is presumably very small, so that the rotation period should be very short, of the order of $P \lessapprox 3$ hr (Pravec et al. 2002). We assume $P = 3$ hr. The exact value of P does not influence the results if the tail age is much longer than that, as can be anticipated from the analysis by Jewitt et al. (2013). The rotation parameters I and Φ are set initially to $I = 0^\circ$ and $\Phi = 0^\circ$. To simplify, we also set all the possible time-variable parameters (except the dust mass loss rate) to a constant value. Thus, the size distribution power index is set to $\alpha = -3.5$, and the minimum and maximum particle sizes to 50 μm and 30 cm, respectively. These values were set after extensive experimentation with the code. Regarding velocities, we employed a function of the kind $v(\beta) = v_0 \beta^\gamma$, where we adopt $\gamma = 1/8$, i.e., a very weak dependence of $v(\beta)$ on β consistent with Moreno et al. (2012a) in their analysis of disrupted asteroid P/2012 F5 (Gibbs). The parameter v_0 and the dust mass loss rate as a function of the heliocentric distance are the fitting parameters.

4. RESULTS

The times of significant dust ejection are first estimated from the best fitting synchrones to the dust tails. This procedure was applied to the *HST* images first, owing to their superb spatial resolution, and then to the GTC images. In the GTC images, the tails named A to F in Jewitt et al. (2013, see Figure 2), the oldest being A, are sometimes blended because of poorer spatial resolution. Thus, in the GTC image of 2013 October 7, we have A, C/B, D, and E/F (see Figure 1). In addition, a younger tail not seen in the *HST* images (named G) appears. On the other hand, the last GTC image of 2013 November 8 does not show the complexity of the others, displaying a single and narrow tail extending to the northeast (see Figure 1). This is surely connected to the fact that the angle between Earth and the asteroid orbital plane (δ) is smaller than at the other dates (see Table 1).

The procedure was then to try different mass loss rates at those times, and set different ejection speeds (distinct v_0) until a good fit to the whole data set (*HST*+GTC) is found in terms of dust tail brightnesses. The synthetic images corresponding to the GTC data are convolved with a point spread Gaussian function in order to take into account the seeing conditions during the observations. During the fitting procedure, we realized that to fit the length of tail "G" in the GTC 2013 October 7 image, we needed to set $r_{\rm min} = 10\,\mu$m at the time of its peak emission, this being the only modification to the particle sizes in the time interval of ejection.

The results of the fits to the *HST* and GTC images are shown in Figures 2 (left panels) and 3. The model reproduces accurately all the features present in the *HST* and GTC images in terms of brightness, length, and width. The dust loss rate profile corresponding to those fits is displayed in Figure 4, resulting in a total dust mass loss of 10^7 kg. The best fitted ejection velocity is given by $v = 0.12\beta^{1/8}$ m s^{-1}. This corresponds to ejection velocities ranging from about 0.02 m s^{-1} to 0.07 m s^{-1}, for 30 cm to 50 μm particles. We have also attempted to fit the images using a constant value for the ejection velocity for all the particles. We found very similar results to those of Figures 2 (left panels) and 3 when a constant ejection velocity in the range 0.02–0.05 m s^{-1} is assumed. Regarding the maximum particle size ejected, we have verified that models having $r_{\rm max} \gtrapprox 1$ cm are compatible with the observations, provided the total mass ejected is modified accordingly. Thus, if $r_{\rm max}$ is set to its lowest acceptable limit, $r_{\rm max} = 1$ cm, the dust mass loss rate would be a factor of ~5 smaller than that shown in Figure 4, i.e., the total dust mass loss would become 2×10^6 kg. This constitutes the lower limit of ejected mass for the assumed particle density of 1000 kg m^{-3} and geometric albedo $p_v = 0.04$.

The range of possible ejection velocities is 0.02–0.05 m s^{-1}. If these values are associated with escape velocities, this translates to possible asteroid diameters (assumed spherical) in the range 30–134 m, and masses in the range 4.6×10^7–1.3×10^9 kg, for assumed bulk densities of 1000–3000 kg m^{-3}. This size estimate is well below the upper limit of 480 ± 80 m diameter derived by Jewitt et al. (2013) on the basis of magnitude measurements of the central condensation. As those authors recognize, this is an upper limit as the measurements could include dust near the nucleus. We believe that it is indeed the case, such that the magnitude of the central condensation is in fact attributable mainly to the dust around the nucleus and not to the nucleus itself, whose contribution must be minimal according to the small size imposed by the escape velocity.

Concerning the rotational parameters of the asteroid, we started, as mentioned, from a scenario in which the rotating axis is perpendicular to the orbit plane ($I = 0^\circ$). We have generated synthetic images by varying both I and Φ in the full ranges, 0°–180°, and 0°–360°, respectively. We found that the only possible fits correspond to obliquities of either $I \sim 0^\circ$ or $I \sim 180^\circ$, independently of Φ, i.e., with the rotating axis nearly perpendicular to the orbit plane, either pointing to the north or the south of the plane (prograde or retrograde motion). When the value of I departs significantly from either 0° or 180°, tails wider than observed are obtained.

Finally, we have also attempted to reproduce the observed brightness pattern using an isotropic ejection model, and the

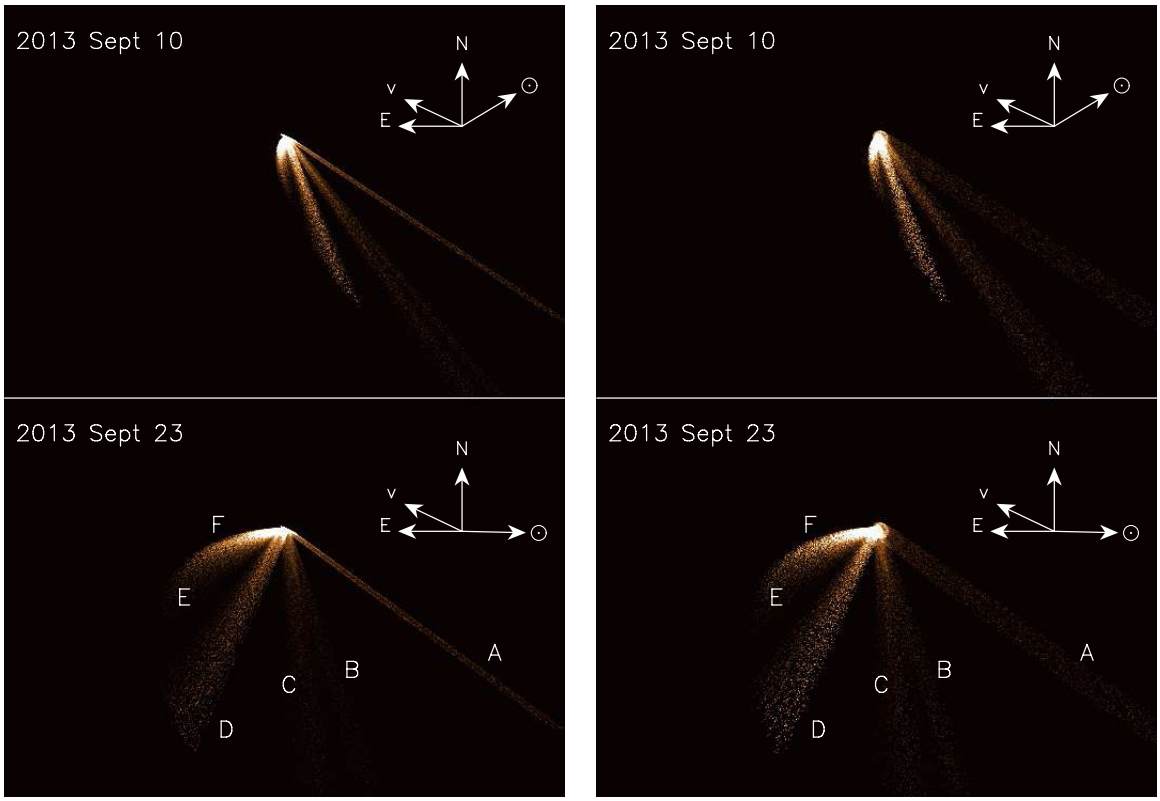

Figure 2. Model simulations of the *Hubble Space Telescope* images by Jewitt et al. (2013, see their Figure 1) at two epochs. The left panels correspond to an anisotropic ejection model, where the particles are ejected from the equator of a rotating nucleus with spin axis perpendicular to the orbit plane. The right panels correspond to an isotropic ejection model, with the same input parameters as the anisotropic model. In the lower panels, each tail is labeled according to the nomenclature by Jewitt et al. (2013). The panels are 23000 km in width, the same as in Figure 1 of Jewitt et al. (2013), to facilitate comparison. The directions of celestial north and east are indicated, as well as the direction to the Sun and the asteroid velocity vector.

(A color version of this figure is available in the online journal.)

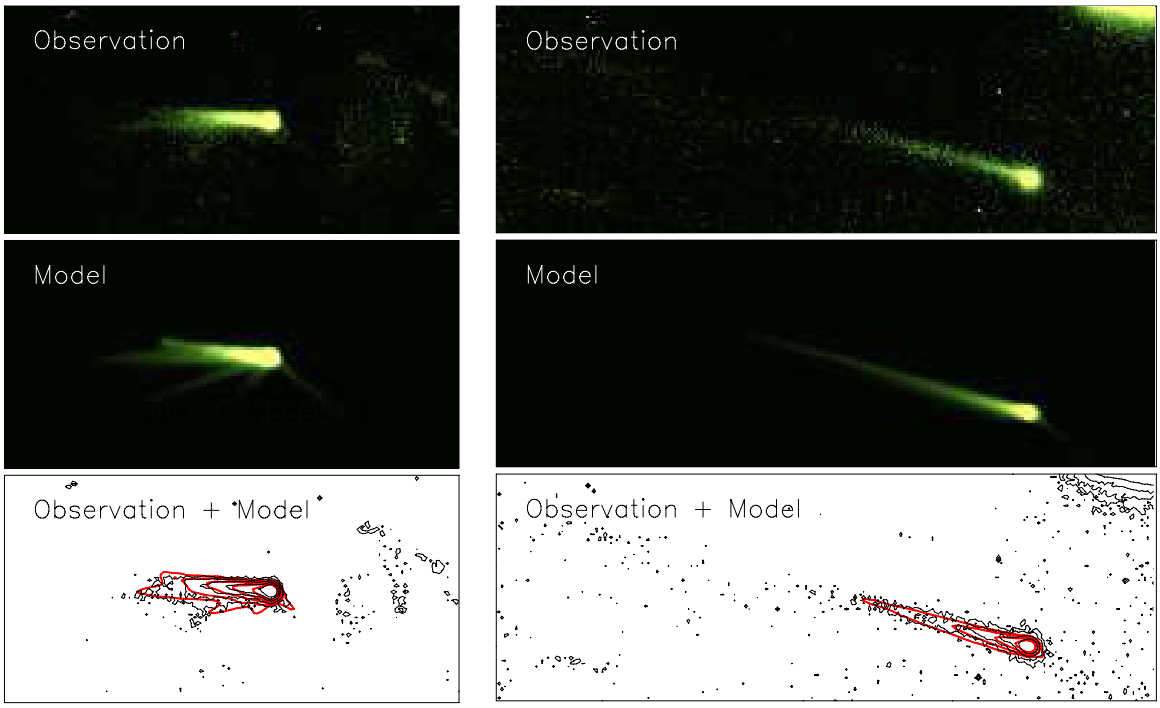

Figure 3. Left panels: observation and model simulation of the 2013 October 7 image. The bottom panel shows the comparison of the observed and modeled isophotes. The innermost isophote level is 3.8×10^{-14} solar disk intensity units, and the isophotes decrease by a factor of two between consecutive levels. Right panels: observation and model simulation of the 2013 November 8 image. The bottom panel shows the comparison of the observed and modeled isophotes. The innermost isophote level is 2×10^{-14} solar disk intensity units, and the isophotes decrease by a factor of two between adjacent levels. The dimensions of the images are the same as in Figure 1.

(A color version of this figure is available in the online journal.)

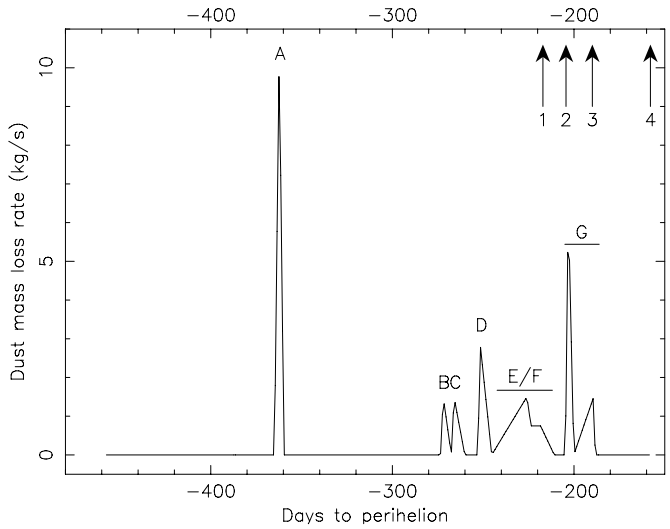

Figure 4. Modeled dust mass loss rate from P/2013 P5 as a function of time to perihelion. The sharp peaks of dust ejection are associated with the tails labeled "A" to "G" (see Figures 2 and 3). The arrows indicate the observation dates of the *HST* (1 and 2) and the GTC (3 and 4) data.

results we obtained for the GTC images are quite similar to those obtained with the above (anisotropic) model. However, the *HST* data are not well reproduced with this isotropic ejection model, as the oldest tails, especially "B," "C," and "A," become significantly broader than observed. This is clearly shown in Figure 2 (right panels).

5. CONCLUSIONS

From the Monte Carlo dust tail modeling of the observations of activated P/2013 P5 (PANSTARRS) we can extract the following conclusions.

1. The object has been subjected to an intermittent dust mass loss, most likely associated with a rotational disruption. This is confirmed from the analysis of both *HST* and GTC images. The total dust mass released was of the order of 10^7 kg, for particle density of 1000 kg m^{-3} and geometric albedo $p_v = 0.04$.
2. The model of rotational disruption, based on simulations of an object that loses mass from its equatorial region, and whose rotational axis is perpendicular to its orbit plane, reproduces to the last detail the observed complex brightness pattern at four different epochs of *HST* and GTC observations. For obliquities different from 0° or 180°, the fits get much worse. On the other hand, an isotropic ejection model does not fit the *HST* data because it produces much more diffuse tails than observed.
3. The ejection velocities are very low, of the order of 0.02–0.05 m s^{-1}. This places the limit on the size of the object to be in the range 30–134 m for assumed densities of 3000–1000 kg m^{-3}.

This article is based on observations made with the Gran Telescopio Canarias (GTC), installed in the Spanish Observatorio del Roque de los Muchachos of the Instituto de Astrofísica de Canarias, in the island of La Palma.

This work was supported by contracts AYA2011-30613-C02-01, AYA2012-39691-C02-01, and FQM-4555 (Proyecto de Excelencia, Junta de Andalucía). J. Licandro acknowledges financial support from the Spanish Ministry of Economy and Competitiveness (MINECO) under the 2011 Severo Ochoa Program MINECO SEV-2011-0187 and AYA2012-39115-C03-03.

REFERENCES

Bertini, I. 2011, P&SS, 59, 365
Bowell, E., Hapke, B., Domingue, D., et al. 1989, in Asteroids II, ed. R. P. Binzel, T. Gehrels, & M. S. Matthews (Tucson, AZ: Univ. Arizona Press), 524
Cepa, J. 2010, in Astrophysics and Space Science Proceedings, Highlights of Spanish Astrophysics V, ed. J. M. Diego, L. J. Goicoechea, & J. Ignacio Gonz (Berlin: Springer), 15
Cepa, J., Aguiar, M., Escalera, V., et al. 2000, Proc. SPIE, 4008, 623
Cox, A. 2000, Allen's Astrophysical Quantities (4th ed., New York: Springer)
Edoh, O. 1983, PhD thesis, Univ. Arizona
Fukugita, M., Ichikawa, T., Gunn, J. E., et al. 1996, AJ, 111, 1748
Fulle, M. 1989, A&A, 217, 283
Fulle, M., Colangeli, L., Agarwal, J., et al. 2010, A&A, 522, 63
Hsieh, H. H., & Jewitt, D. 2006, Sci, 312, 561
Jewitt, D. 2012, AJ, 143, 21
Jewitt, D., Agarwal, J., Weaver, H., et al. 2013, ApJL, 778, L21
Jewitt, D., Weaver, H., Agarwal, J., et al. 2010, Natur, 467, 817
Masiero, J. R., Mainzer, A. K., Bauer, J. M., et al. 2013, ApJ, 770, 7
Micheli, M., Tholen, D. J., Primak, N., et al. 2013, MPEC, 2013-Q37
Moreno, F., Licandro, J., & Cabrera-Lavers, A. 2012a, ApJL, 761, L12
Moreno, F., Licandro, J., & Ortiz, J. L. 2013, ApJ, submitted
Moreno, F., Licandro, J., Tozzi, G.-P., et al. 2010, ApJL, 718, L132
Moreno, F., Pozuelos, F., Aceituno, F., et al. 2012b, ApJ, 752, 136
Pravec, P., Harris, A. W., & Michalowski, T. 2002, in Asteroids III, ed. W. F. Bottke, A. Cellino, P. Paolicchi, & R. Binzel (Tucson, AZ: Univ. of Arizona Press), 113
Snodgrass, C., Tubiana, C., Vincent, J.-B., et al. 2010, Natur, 467, 814